

Exploring glassy dynamics with Markov state models from graph dynamical neural networks

Siavash Soltani,¹ Chad W. Sinclair,¹ and Jörg Rottler^{2,3}

¹*Department of Materials Engineering, The University of British Columbia, Vancouver, BC, Canada V6T 1Z4*

²*Department of Physics and Astronomy, The University of British Columbia, Vancouver, BC, Canada V6T 1Z1*

³*Stewart Blusson Quantum Matter Institute, The University of British Columbia, Vancouver, BC, Canada V6T 1Z4*

Amorphous materials exhibit structural heterogeneities that relax only on long timescales. Using machine learning techniques, we construct a Markov state model (MSM) for model glass formers that coarse-grains the dynamics into a low-dimensional space, in which transitions occur with rates corresponding to the slowest modes of the system. The transition timescale between states is more than an order of magnitude larger than the conventional alpha-relaxation time, and reveals a fragile to strong crossover at the glass transition. The learned map of states assigned to the particles exhibits correlations of a few molecular diameters both at liquid and glassy temperatures. We show that the MSM effectively constructs a map of scaled excess Voronoi volume, and the free energy difference between the two states is given exactly by the entropy of these distributions. These results resonate with classic free volume theories of the glass transition, singling out local packing fluctuations as the slowest relaxing features.

Establishing robust links between the structural and dynamical heterogeneity found in amorphous materials at the nanoscale is notoriously difficult due to the complex local environment of constituent particles [1–5]. Structural indicators such as local density, bond order, atomic Voronoi volumes, potential energy, or linear response quantities such as local shear moduli all exhibit broadly peaked distributions, and their spatial maps reveal features with correlation lengths of order a few particle diameters. At the same time, maps of the squared displacement of particles partition space into fast and slow moving regions, with dynamical correlation lengths growing weakly upon approach to the glass transition [6].

Machine learning (ML) techniques have proven useful in the quest for understanding structure-dynamics relationships due to their powerful capabilities in dimensionality reduction and extracting dominant structural features [7–9]. Support vector machines (SVMs) can be trained on local structural features in order to assign a ‘softness’ value to each particle that predicts a dynamical property such as its probability of rearrangement [10–14]. Replacing SVM’s with graph neural networks [15] obviates the need for pre-determined feature functions as they can be updated during the training of the model, resulting in a more accurate representation of the local atomistic environment and improved prediction accuracy. Unsupervised learning approaches based on autoencoders [16] or information-theoretic inference of communities [17] require only structural information as input and assign a binary or continuous variable to particles that was found to correlate with measures of their mobility in the supercooled regime.

The unsupervised ML methods proposed so far all aim to classify particles based on structural information alone. What is needed is a method that treats structure and dynamics on the same footing by analysing directly the molecular trajectories, ‘automatically’ identifying the rate limiting processes and then associating particles to the corresponding spatial features. In this way, one can

hope to simultaneously identify the relevant hydrodynamic variables and their relaxation timescales. Exactly such a program is offered by Markov state models [18]. Importantly, MSMs enable one to extract dynamical information from an ensemble of trajectories each much shorter than the timescale of interest. These models have a long tradition in molecular biophysics [19–21], where they are used to capture slow conformational changes of proteins and biomolecules that occur far beyond the nanosecond timescales of direct MD simulations [22]. Major progress occurred with the introduction of the variational principle for Markov processes (VAMP) [23], which when combined with deep learning methods permits the automated construction of MSMs from molecular trajectories [24].

The VAMP formulation of MSMs has been combined recently with graph dynamical networks (GDyNets) in order to infer the dynamics of atomic scale processes in various condensed matter systems [25]. In this method, the local environment of particles is mapped into a state space where the dynamics are linear, and the time scale of the limiting processes are extracted using MSMs directly trained on the dynamics of particles. Here, we use VAMP/GDyNets based MSMs to study the long time dynamics of a model glass forming liquid over a wide range of temperatures ranging from the liquid state down to deep in the glassy regime, where standard analysis of dynamics is extremely challenging. We construct a two-state Markov state model that reveals relaxation processes on diffusive timescales, much longer than the main structural α -relaxation time that is conventionally used to characterize glassy dynamics. The conversion timescale τ_{MSM} between the two states has a super-Arrhenius temperature dependence above the glass transition, but crosses over into simple Arrhenius behavior at low temperatures. The transitions between the states identified by our MSM describe local excess volume fluctuations. As assumed in classical free volume theories of the glass transition, the free energy difference

between these states is purely entropic. The two-state map correlates strongly with the dynamical propensity evaluated at τ_{MSM} and also predicts local regions with a high probability of rearrangements. The MSM viewpoint of glassy dynamics thus identifies local packing fluctuations as the slowest relaxing structural observable.

Results

Two-state Markov model. In Markov models, the state space of the system is discretized, and it is assumed that the state at time $t + \delta t$ only depends on the state at time t . The time evolution of the system is then captured by the transition matrix, $\mathbf{K}(\delta t)$ that propagates the probability vector of finding the system in a given state. Elements of the transition matrix $K_{ij}(\delta t)$ are the probabilities of observing the system in state j at $t = t + \delta t$ given that the system was in state i at time t . The optimal feature map functions that assign this probability to each particle are learned from molecular dynamics trajectories with graph convolutional networks as described in Methods and in refs. [24, 25].

A two-state Markov model is completely defined by the conversion rates $k_{0 \rightarrow 1}$ and $k_{1 \rightarrow 0}$ between states 0 and 1. The nontrivial eigenvalue λ_2 of the transition matrix $\mathbf{K}(\delta t)$ determines the total conversion timescale,

$$\tau_{MSM} = -\frac{\delta t}{\ln |\lambda_2|} = \frac{1}{k_{0 \rightarrow 1} + k_{1 \rightarrow 0}}. \quad (1)$$

If the process is Markovian, τ_{MSM} does not depend on the choice of δt . Therefore, to test the convergence to Markovianity, one should approximate τ_{MSM} as a function of lag time δt , see Supplementary Figure 1.

The equilibrium distribution (eigenvector associated with $\lambda_1 = 1$) is given by

$$v_1 = \left(\frac{k_{1 \rightarrow 0}}{k_{0 \rightarrow 1} + k_{1 \rightarrow 0}}, \frac{k_{0 \rightarrow 1}}{k_{0 \rightarrow 1} + k_{1 \rightarrow 0}} \right). \quad (2)$$

We focus on the simulation of an extremely well characterized model glass former, namely N=40,000 particles of a 80-20 binary Lennard-Jones mixture in a periodic simulation box at various temperatures ranging from $T = 0.25$ to $T = 1$ (all quantities are given in reduced units). To confirm robustness of the results and check the role of dimensionality, a parallel study of a two-dimensional (2D) 65-35 binary Lennard-Jones mixture was made. As the findings are qualitatively similar, we relegate the results for the 2D system to Supplementary Information. Feature map functions are trained on the trajectories of the majority particles at temperature $T = 0.4$, and we then extract the relaxation time of the Markov process τ_{MSM} across all temperatures. Results are shown in Fig. 1a in an Arrhenius representation. In all cases, the lag time δt is large enough for τ_{MSM} to be independent of δt (see Supplementary Figure 1). The conventional α -relaxation times extracted from the decay of the self-intermediate scattering function $F_s(\mathbf{q}, t) = 1/N \sum_i^N \cos[\mathbf{q}(\mathbf{r}_i(t) - \mathbf{r}_i(0))]$ to $1/e$ for

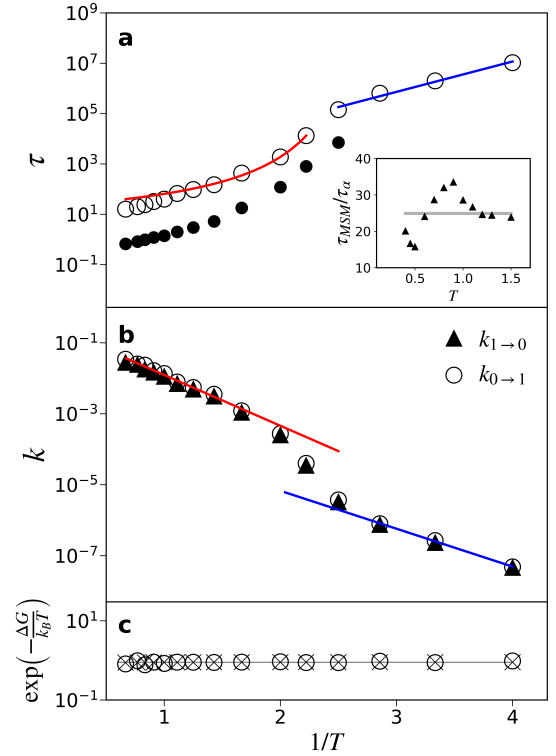


Fig. 1 Relaxation times, forward and backward reaction rates and free energies obtained using Markov state model. **a** Markov state relaxation times (empty circles) and α relaxation time (filled circles) as a function of inverse temperature. Red solid curve shows a Vogel-Fulcher-Tammann fit, $\tau \sim \exp[A/(T - T_0)]$ of the data for $T \geq 0.45$. The obtained T_0 value is 0.34. An Arrhenius fit at low temperatures is also shown with a blue solid line. **b** Forward and backward reaction rates, $k_{0 \rightarrow 1}$ and $k_{1 \rightarrow 0}$. **c** Free energy difference between states (circles), see Eq. (3) and $\exp(-\Delta S/k_B)$ (\times) see Eq. (6).

$|\mathbf{q}| = 7.2$ are also shown for temperatures in the fluid and supercooled regime $T \geq 0.4$, where they can be computed. For these temperatures, the MSM time appears to be roughly proportional to the α -relaxation time but is at least an order of magnitude longer. This suggests that the process identified by the Markov model as rate limiting is not the α -relaxation itself, but a transition which takes places over longer time scales than cage-breaking rearrangements. In this regime, the temperature dependence can be fit with a Vogel-Fulcher-Tammann (VFT) law. However, the MSM model can be constructed for lower temperatures deep in the glassy regime $T \leq 0.4$, where it reveals a crossover from the well-known super-Arrhenius behavior above the glass transition to purely Arrhenius behavior below $T_c \approx 0.435$. The inset reveals that both in the fluid and glassy regimes, the ratio of MSM to α time scales is about 25 (approx. 300 in the 2D model, see Supplementary Figure 2.). Some variation is

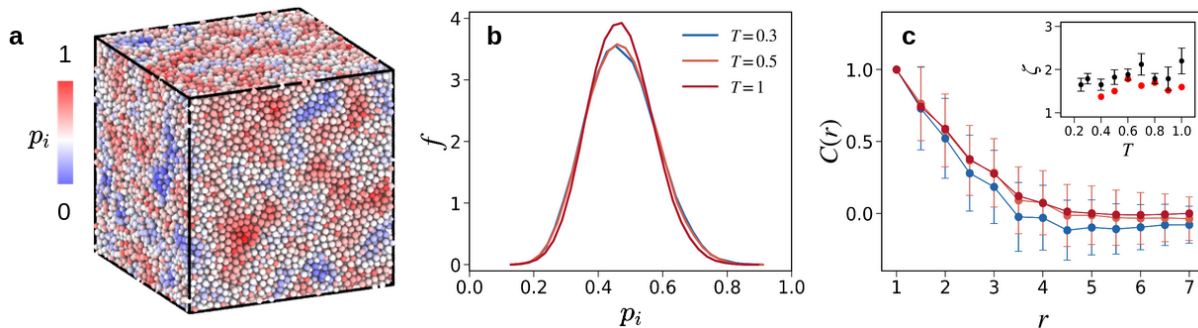


Fig. 2 Structural analysis of state maps. **a** Example of a state map at $T=0.3$. Particles are colored according to their probability of being in state 0, assigned by the graph dynamical network. **b** Probability distribution of the majority type particles of being in state 0 at 3 different temperatures. Distributions are averaged over 100 equally spaced snapshots of the trajectory. **c** Normalized spatial correlation functions $C(r) = \langle \delta p(0) \delta p(r) \rangle / \langle \delta p(0) \delta p(r_{min}) \rangle$ of the state maps at same temperatures as in panel **b**. Measurements are obtained using 5 different quench realizations to desired temperatures and an iso-thermal equilibration of 50,000 LJ time. The snapshot at the end of this equilibration period is then used to extract the data points in **c**. The error bars show the standard error of the mean. Black symbols in inset show the correlation length of the state map, ζ calculated using Eq. (5). Red symbols represent RMSD of all particles at $t = \tau_{MSM}$. Error bars in the inset show the standard error of the mean. Visualizations are performed using Ovito [26].

observed for intermediate temperatures, indicating that here the free energy barriers for the two processes differ slightly while being similar at fluid and energy landscape dominated (i.e. glassy) temperatures.

Writing the rates in the form $k_{i \rightarrow j} = \tau_0^{-1} \exp[-(G^* - G_i)/k_B T]$, where G_i and G^* denote the free energies in state i and in the transition state, we can interpret the two-state model in an energy landscape picture. According to equations (1) and (2), the rates themselves can be obtained by dividing the components of the eigenvector v_1 by τ_{MSM} , while the free energy difference between the two states can be inferred from the ratio of the eigenvector components (assuming the same pref-factor),

$$\frac{k_{0 \rightarrow 1}}{k_{1 \rightarrow 0}} \approx e^{-(G_2 - G_1)/k_B T}. \quad (3)$$

In Fig. 1b we show the ‘forward’ and ‘backward’ reaction rates $k_{0 \rightarrow 1}$ and $k_{1 \rightarrow 0}$, respectively. The rates almost trace each other, which suggests a very small free energy difference between the states. An Arrhenius fit to the high temperature regime reveals an activation barrier of 3.29 LJ energy units, together with a pre-exponential factor $\tau_0 \approx 1$. In the fluid, we expect indeed an attempt frequency of order an atomic vibration (Einstein) frequency. The barrier then rises strongly as the temperature drops, signalling the approaching glass transition. Deep in the glassy state, the barrier becomes temperature independent again and settles on a somewhat smaller value of 2.46 LJ energy units, but the pre-exponential time is now about a factor 1000 larger. This behavior signals a large entropic penalty for rearrangement, in agreement with the notion that cooperative motion of many particles is now needed for relaxation to occur.

A final insight that can be obtained from the

transition matrix concerns the free energy difference $\Delta G = G_2 - G_1$ between the states. Fig. 1c shows that $\exp[-\Delta G/k_B T]$ is temperature independent, from which we infer $\Delta G = 0.1 k_B T$. The linear temperature dependence implies that ΔG is also entropic in origin.

Heterogeneous state maps. Fig. 2a shows the output of the graph dynamical network for snapshots of the simulation in the glassy regime. Since the number of states is defined to be two, the network assigns a probability p_i to each particle i which denotes how similar the local environment of a particle is to state 0. Distinct clusters of particles in the same state emerge, reflecting a form of heterogeneity. For this projection, a separate network was trained on the dynamics of the minority particles. The assigned states merge seamlessly into those for the majority particles, while τ_{MSM} is identical (training on all particles simultaneously in the binary mixture results in a trivial partitioning by chemical identity). The timescale, τ_{MSM} , can also be thought of as the time required for the distribution of p_i to spatially de-correlate.

The histograms of the state probabilities of the majority particles in Fig. 2b reveal broadly peaked distributions that are insensitive to temperature. The average probability 0.47 agrees well with the value of the (also temperature insensitive) eigenvector component, which corresponds to the equilibrium distribution of the two-state model. These results suggest that the distributions in Fig. 2b represent equilibrium configurations, which they can presumably reach at high temperature where τ_{MSM} is small. The heterogeneous state maps from our MSM bears superficial similarity with the maps of a scalar structural order parameter P obtained by Boatini et al. [16], who encoded the local atomic environment

in to bond order parameters and classified them using a neural network auto-encoder. However, the mean of this order parameter $\langle P \rangle$ decreases with increasing temperature, while $\langle p_i \rangle$ does not.

In order to measure the size of the features, we first calculate normalized fluctuations in the state map,

$$\delta p_i = \frac{p_i - \langle p \rangle}{\sqrt{\langle (p - \langle p \rangle)^2 \rangle}} \quad (4)$$

The correlation function $C(r) = \langle \delta p(0) \delta p(r) \rangle / \langle \delta p(0) \delta p(r_{min}) \rangle$ is then calculated, where the average is over all particles separated by a distance r and $r_{min} = 1$. Fig. 2c shows typical correlation functions as a function of r . We then calculate the correlation length ζ as

$$\zeta = \frac{\sum_{r=r_{min}}^{r_{cut}} \langle \delta p(0) \delta p(r) \rangle \delta r}{\sum_{r=r_{min}}^{r_{cut}} \langle \delta p(0) \delta p(r) \rangle}. \quad (5)$$

Here δr and r_{cut} were chosen to be 0.5 and 7 respectively. The inset of panel (c) shows the correlation length in the state map, averaged over 5 different initial configurations quenched at the same rate and equilibrated at the desired temperatures. The length scale of features in the state maps averages around 1.8 (around 3.5 in the 2D model, see Supplementary Figure 3.) and is insensitive to temperature. The Markov states are thus larger than soft spots, for which a correlation length of order one particle diameter has been reported [12]. Accordingly, one expects the lifetimes of the soft spots to be shorter. For comparison, the root-mean-squared displacements (RMSD) of all particles evaluated at $t = \tau_{MSM}$ are also shown in the inset, and agree well with the correlation length. This suggests that the MSM timescale corresponds to the time for particles to diffuse over the feature size, which is consistent with the interpretation of the MSM timescale as being the transformation time between states.

Having the state of particles, we can calculate the entropy of the distributions of each of the two states using Gibbs' formula,

$$S_j = -k_B \sum_{i=1}^{N_A} p_i^j \ln p_i^j \quad (6)$$

where p_i^j is the probability of observing particle i in state $j = 0, 1$, and N_A is the number of particles type A . If the free energy difference $\Delta G = \Delta H - T\Delta S$ between the two states is purely entropic, $\exp(-\Delta S/k_B) = v_1^{(1)}/v_1^{(2)}$ where $v_1^{(1)}$ and $v_1^{(2)}$ are the elements of the first eigenvector of the transition matrix and $\Delta S = S_0 - S_1$. Fig. 1c shows that the above equality is indeed fulfilled for all temperatures studied.

Interpretation of the state map. The question is now what dynamic process the VAMP/GDyNet identifies as the slowest (i.e. hydrodynamic) mode of relaxation of

the system? We find that there is a strong correlation between the state map (composed of majority particles) and local excess Voronoi volume of the same particles. To quantify this correlation, we use the Pearson correlation factor

$$\rho = \frac{\sum_{i=0}^{N_A} (p_i - \bar{p})(v_i - \bar{v})}{\sqrt{\sum_{i=0}^{N_A} (p_i - \bar{p})^2} \sqrt{\sum_{i=0}^{N_A} (v_i - \bar{v})^2}}, \quad (7)$$

where p_i is the state of the particle and v_i the Voronoi cell volume of particle i . The Pearson correlation factor, ρ , calculated between two quantities ranges between -1 and 1, with $\rho = 0$ indicating no correlations. The Pearson correlation between state maps and maps of local Voronoi volumes is near 0.5 for all temperatures. In order to reduce the inherent noise in the site-to-site variation of Voronoi volumes, we also consider a lightly coarse-grained map of Voronoi volumes, $v_{i,s}$, by averaging over particles within a range $r = \zeta$, where ζ is the correlation length in the state map, see Fig. 2c. This local smoothing significantly increases the Pearson factor to 0.84. Such high values imply nearly identical configurations, as can be confirmed by visual inspection of two example maps in Fig. 3a.

In order to compare the distributions of state probability and coarse-grained Voronoi volumes quantitatively, we scale volumes to:

$$\tilde{v}_{i,s} = (v_{i,s} - v_{s,min}) / (v_{s,max} - v_{s,min}) \quad (8)$$

which can be interpreted as an excess volume with values ranging between zero and one. Fig. 3b shows that these distributions indeed overlap to an excellent degree. Fig. 3c further illustrates the link between Markov states and local excess volume in the form of a nearly linear relationship between the two variables. It can be expected that majority particles in state 1 that have a small Voronoi volume around them also have many minority particles around them. This trend is also borne out in Fig. 3c, which shows that the number density n_B of the minority (B) particles anticorrelates with the scaled Voronoi volume of the majority particles. n_B for each particle is defined as the ratio of number of B neighbors divided by the total number of neighbors within $r_c = 2.5$, where r_c is the location of the second minimum in the radial distribution function.

The equivalence of the distributions of the state probabilities and excess Voronoi volumes implies that the entropy difference between the two states can also be interpreted as an entropy difference of Voronoi cell volumes. This finding resonates with classic free volume theories of the glass transition. For instance, Cohen and Grest [27] define a local free volume as $v_f = v - v_c$, where v_c is a critical volume that separates cells into liquid like and solid like cells, and the entropy of the probability distribution is the only contribution to the free energy change involved in redistributing free volume. In close analogy, our MSM describes transitions between regions of high and low excess free volume, and yields a purely

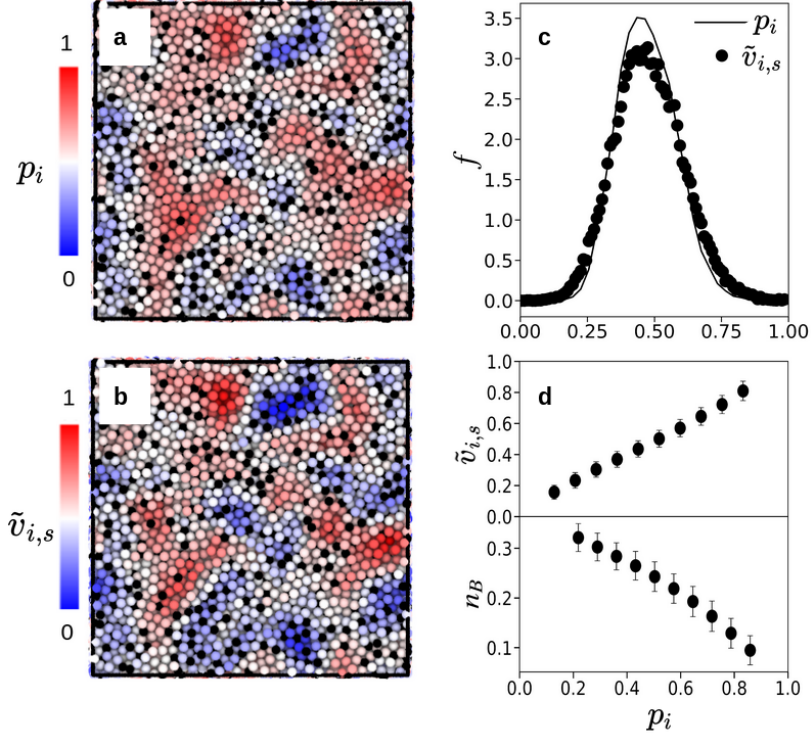


Fig. 3 Correlation between the state map and structural and chemical properties. Comparison between **a** state map of majority particles and **b** coarse grained and scaled Voronoi volume. Voronoi volume of particles are lightly smoothed by averaging the Voronoi volume of a particle with its neighbors within $r = \zeta$, for a snapshot at $T = 0.4$ and are then scaled to range between 0 and 1 using Eq. (8). Minority particles are shown in black. **c** Comparison between the distribution of states and $\tilde{v}_{i,s}$. **d** mean Voronoi volume and number density of minority (B) particles versus state probability. Error bars show the standard error of the mean.

entropic free energy difference between these regions.

Relationship to local dynamics. Further insight into the nature of the states identified by the MSM can be gleaned from a comparison with the dynamic propensity [28]. This quantity is a measure of structural heterogeneity in disordered packings and is computed in the ‘isoconfigurational ensemble’; the squared displacement of a particle is averaged over a number of simulations that originate in the same configuration but differ only in their initial velocities. Correlations between dynamic propensity and local density have been observed elsewhere [15], where it has been shown that a graph network trained to predict propensity provides a coarse description of local density of particles.

Here we explore the relationship between dynamic propensity and the state map obtained from the GDyNets. We perform 10 isoconfigurational MD runs starting from the saved configurations at desired temperatures during the quench with random initialization of velocities to obtain the average squared displacement of each particle (the propensity) as a function of time. The correlation between the state map computed at time zero and propensity at time t are again characterized using the Pearson correlation factor, see Fig. 4a. A peak in the

correlation is observed at each temperature and close to the estimated time scale of the MSM, see Fig. 1a. Keeping in mind the link between states and local Voronoi volumes, this result is perfectly consistent with two earlier studies that reported maximal correlations between lightly coarse grained local density and the propensity at approximately $20 - 30\tau_\alpha$ in the same model glass [17, 29]. It also shows that the MSM state map is distinct from the scalar order parameter map of Boattini et al. [16], which, like softness [11, 15], correlates maximally with the propensity at τ_α . Note that the MSM was not trained to predict the propensity, yet the correlation of the state map and propensity at $t = \tau_{MSM}$ is comparable with a recent study [15], where the target of the model was to predict the propensity of particles. An advantage of the unsupervised learning method used here is that it additionally gives the time scale of transitions between states.

The original motivation behind the soft spot concept was to be able to predict where local shear transformations are more likely to occur in a homogeneous disordered packing. Schoenholz et al. have found that fluctuations in local density have the most influence on softness [11], and that softness decreases with increasing coordination number [12]. Specifically, the most

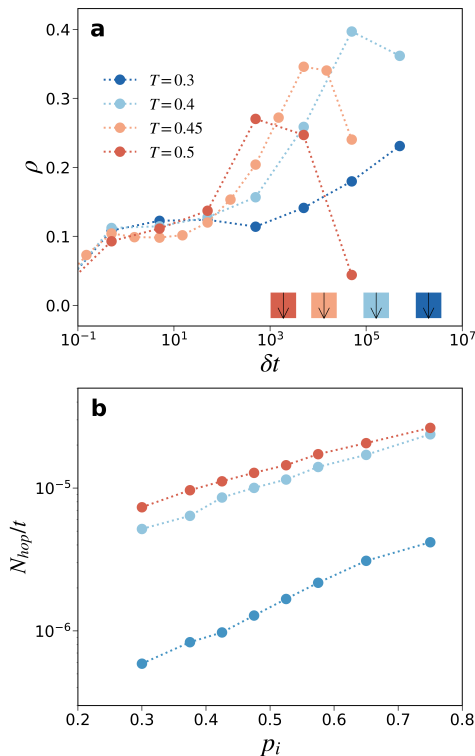


Fig. 4 Correlation between the state map and dynamics. **a** Pearson correlation coefficient between state map and dynamic propensity at 4 different temperatures. The state map is obtained using the snapshot immediately after quench, and the propensity is evaluated as a function of lag time δt from this snapshot. Arrows at the bottom show the MSM time scale τ_{MSM} for each temperature. **b** Average number of hops per unit time vs. the state variable for three different temperatures, $T=0.35$, 0.4 and 0.5 . Jump rates are normalized with respect to the overall state probability distributions.

important structural feature that captures softness is the density of particles at the first peak of the radial distribution function [11]. Since the MSM state map developed here reflects such local packing fluctuations, is it natural to expect that the state map is also capable of predicting rearrangements. To test this idea, we identify individual hops or jumps of particles using established methods [30, 31] (see Methods) and consider these as elementary rearrangements. Fig. 4b shows that the probability of rearrangements increases monotonically with the state variable. Particles in state 0 rearrange at a rate about one order magnitude greater than particles in state 1. This behavior mirrors that found for soft spots [11], albeit somewhat less pronounced. This is not surprising, given that past work has shown that a combination of features is needed to optimally predict local rearrangements.

Discussion

We have introduced a two-state Markov model for the study of slow dynamics in glassy systems using unsupervised machine learning techniques. Following earlier work [24, 25], feature map functions were learned with graph dynamical networks (GDyNets) in combination with the variational approach for Markov processes (VAMP). The graph neural network proves to be a powerful and effective method to map the complicated local environment of particles to a state space with low dimensions, resulting in a coarse-grained description of dynamics. In model glass formers in two and three dimensions, the algorithm reveals a heterogeneous map, where particles are classified according to their local excess Voronoi volumes. The free energy difference between the two states was found to be proportional to temperature, implying that it results from entropy differences between the two states. Since the dynamics are linear in the state space, the relaxation towards equilibrium is purely exponential, enabling us to extract the timescales from short trajectories.

Despite being globally isotropic, amorphous solids exhibit structural heterogeneity at the nanoscale. As a key insight of this work, the structurally agnostic GDyNets selects transitions between regions of high and low excess Voronoi volume as the slowest mode of relaxation that can be considered Markovian. The timescale of transitions between these regions is more than an order of magnitude larger than the structural α -relaxation time. Such a proportionality might be expected for simple diffusive processes. A prediction of this work is that local excess volume fluctuations are the longest living features (i.e. the most important hydrodynamic variable) in the glass, and all other structural heterogeneities should equilibrate faster. Importantly, the structural heterogeneities are measurable at all temperatures, whereas dynamical heterogeneities disappear in the fluid regime.

In contrast to softness methods, where the model is directly trained to predict rearrangements [10] or propensity [15] of particles by supervised learning, the MSM in this work is not trained on these dynamical properties. Our approach is also philosophically distinct from recent unsupervised learning approaches [16, 17] that use structural information alone to establish links between local order and dynamics in the supercooled regime. By including the observed dynamics, our approach instead constructs a kinetic model applicable to all temperatures that makes predictions about the thermodynamics of the underlying two-state system. The model predicts the dynamic propensity [28] evaluated at the intrinsic MSM timescale, and also to some degree the rearrangement of particles. Since the VAMP/GDyNets approach is an unsupervised learning process, the dynamical heterogeneity is therefore truly emergent and not fed into the model. The correlation length in the state map was found to be larger than those found in softness methods, pointing towards the idea that the local structure and dynamics of particles are even further correlated in space than one

might infer from the typical size of soft spots.

An important advantage of the MSM is that MD simulations can be pushed deep into the glassy regime where correlation functions probing longer length scales decay too slowly to extract timescales or rearrangements occur too infrequently to learn a softness field. Here we were able to observe very clearly the crossover from VFT behavior to simple Arrhenius dynamics below the glass transition in the 65-35 (2D) and 80-20 (3D) binary Lennard-Jones mixture. Such changes in fragility are also seen in many amorphous metals and polymers, often occurring already in the supercooled regime above T_g [32, 33].

VAMP/GDyNets can be applied to a variety of problems to understand the complicated dynamics in glassy systems under different thermodynamic and mechanical conditions. For example, an interesting topic for future work might be to study the effects of aging on the MSM time scale, or the accelerated dynamics of the state map relaxation under various forms of deformation.

Methods

Markov State Models. Markov State Models discretize state space assuming that the state of the system at time $t + \delta t$ only depends on the state at time t and not previous times. The time evolution of the system is then captured by the transition matrix, $\mathbf{K}(\delta t)$:

$$\mathbf{P}(t + \delta t) = \mathbf{K}(\delta t)^T \mathbf{P}(t) \quad (9)$$

where $\mathbf{P}(t)$ is a vector whose elements are the probability of finding the system in state i at time t . Elements of the transition matrix $\mathbf{K}_{ij}(\delta t)$ are the probabilities of observing the system in state j at $t = t + \delta t$ given that the system was in state i at time t . If the system has a unique equilibrium distribution, the eigenvalues of the transition matrix have the form $|\lambda_i| \leq 1$. There is exactly one eigenvalue equal to 1 and the corresponding eigenvector represents the equilibrium distribution since the application of the transition matrix leaves this vector unchanged. Moreover, the eigenvalues of the transition matrix are real and eigenvectors form a complete set. The result is that the temporal evolution of the system in state space can be described by i dynamic modes, each decaying exponentially with a characteristic relaxation time as described by Eq. (1).

If the kinetics are Markovian, $\tau_{MSM}(\delta t)$ does not depend on the choice of δt . Therefore, to test the convergence to Markovianity, one should approximate τ_{MSM} as a function of lag time δt . For the situation studied here where our states are comprised of many lumped states, achieving Markovianity will require some finite δt so testing the evolution of τ_{MSM} as a function of δt is important [19].

Finally, to test the accuracy of any Markov State model, one can estimate a transition matrix at lag times $n\delta t$, and perform a Chapman-Kolmogorov (CK) test [24],

$$\mathbf{K}(n\delta t) = \mathbf{K}^n(\delta t). \quad (10)$$

This must hold within statistical uncertainty. For all cases studied here this test was performed, results being given in Supplementary Information. For more information on generation and validation of Markov state models the reader is referred to [20, 34, 35].

Constructing Markov State Models using Graph dynamical networks (GDyNets) optimized by VAMPs. In order to construct an efficient Markov state model from a molecular dynamics trajectory, it is necessary to reduce the system dimensionality, grouping together atoms with similar structural and dynamical features into ‘states’. While in some cases the identification of these ‘states’ is trivial, in cases like the one studied here it is not. Thus, the first step required is to identify so-called feature map functions, $\chi(\mathbf{x}_t)$ where \mathbf{x}_t represents the local configurations of atoms at time t . These feature map functions then produce the vectors $\mathbf{P}(t)$ and $\mathbf{P}(t + \delta t)$ used in Eq. (9) from input time series snapshots of molecular dynamics trajectories.

To facilitate the training of the feature map functions, we have employed the GDyNets methodology originally proposed in ref. [25]. Here, we give only a short explanation focusing on details of our implementation. The GDyNet constructs graphs of input configurations for MD snapshot it is provided. Each particle is represented by a node q_i , which is initialized randomly according to the particle type and is a vector with a pre-defined length (64 here). Note that the local chemical environment of particles is also taken into account in feature vectors, unlike softness models where features are defined solely based on structure. The edges of the graph are determined by using the radial structure functions of 20 nearest neighbors of the target particle i ,

$$u_{(i,j)} = \exp(-(d_{(i,j)} - \mu_n)^2 / \gamma^2), \quad (11)$$

where $d_{(i,j)}$ denotes the distance between particle i and its neighbor j , $\gamma = 0.2$, $\mu_n = 0.2n$ for $n = 0, 1, 2, \dots, 35$. Therefore for each neighbor, μ_n changes from 0 to 7 resulting in a vector $u_{(i,j)}$ with length 36.

The same hyperparameters as in ref. [25] are used. For each node, the vectors $q_i^{(l-1)}$, $q_j^{(l-1)}$ and $u_{(i,j)}$ from the last iteration are then concatenated:

$$z_{(i,j)}^{(l-1)} = q_i^{(l-1)} \oplus q_j^{(l-1)} \oplus u_{(i,j)}. \quad (12)$$

A scalar, α_{ij} is also calculated for each neighbor:

$$\alpha_{ij} = \frac{\exp(z_{(i,j)}^{(l-1)} W_a^{(l-1)} + b_a^{(l-1)})}{\sum_j \exp(z_{(i,j)}^{(l-1)} W_a^{(l-1)} + b_a^{(l-1)})}, \quad (13)$$

which is called the attention coefficient of each neighbor. The embedding of node i is then updated using convolution:

$$q_i^{(l)} = q_i^{(l-1)} + \sum_j \alpha_{ij} \cdot g(z_{(i,j)}^{(l-1)} W_n^{(l-1)} + b_n^{(l-1)}) \quad (14)$$

In this work, we use $l = 3$ convolutional layers. W_n and b_n are the weight and biases of the layer and g is the ReLU activation function. Note that without the attention layer, all neighbors share the same weight and bias matrices, W_n and b_n , which neglects the differences of interaction strength between neighbors [25]. By convolution, information from particles beyond the first neighbor shell also reach the target particle. The final output of this convolutional network, q_i^l at times t and $t + \delta t$ are therefore the embeddings of atom i at times t and $t + \delta t$. These results are passed to a two-layer fully-connected neural network with a Softmax activation layer in order to compute the final probability of each atom to belong to state 0 and 1. Note that this two-layer network is computed using the basic framework described in [24].

While it would be attractive to use minimize of the least square error, $\|\chi(\mathbf{x}_{t+\delta t}) - \mathbf{K}^T \chi(\mathbf{x}_t)\|^2$ as the metric against which the network can be trained, it has been shown that this is not robust [24]. Rather, Noé and co-workers have proposed the concept of the variational approach for Markov processes (VAMP) [23, 24]. Here, the network has been trained to maximize the so-called VAMP-2 score based on covariance matrices obtained from the feature mapping provided by the above network at times \mathbf{x}_t and $\mathbf{x}_{t+\delta t}$ [24]. In this way the entire trajectory can be used to optimize the network simultaneously.

To study the dynamics in a wide range of temperatures, we have trained our network using the simulation trajectories of particles of type A (the majority particles) and type B at $T = 0.4$ for both 2d and 3d systems. This trained model was then applied to simulation data obtained at other temperatures. This ensures that the transformation function χ are similar for all temperatures. We chose $T = 0.4$ to train the model to test the ability of the method to efficiently identify dynamic processes at temperatures where kinetics are slow. The hyperparameter δt is chosen to be $25\tau_{LJ}$ for the 2d system and $200\tau_{LJ}$ for the 3d system, about 10 times and 30 times smaller than the α -relaxation times at $T = 0.4$. To analyze the trajectories using VAMP/GDyNets, construct the MSMs and extract τ_{MSM} , the codes from [36] were used.

Glass models and molecular dynamics simulations. Two standard glass forming binary liquids are studied with molecular dynamics simulations using LAMMPS. The 3-dimensional Kob-Andersen (KA) Lennard-Jones system with the composition 80-20 serves as the main model system detailed in the body of the paper. A two-dimensional model with the composition 65-35 was also studied but found to provide qualitatively the same results. Detailed results from the two-dimensional model are made available as Supplementary Information. The interaction potential is $V_{\alpha\beta} = 4\epsilon_{\alpha\beta}[(\sigma_{\alpha\beta}/r)^{12} - (\sigma_{\alpha\beta}/r)^6]$ where $\epsilon_{BB} = 0.5$, $\epsilon_{AB} = 1.5$, $\sigma_{BB} = 0.88$ and $\sigma_{AB} = 0.88$. We ignore interactions with $r > 2.5\sigma_{AA}$. The 3D system has a

total of 40,000 particles of type A and B in a simulation box with length of 32.18 particle diameters in x,y and z directions. The 2D system contains 50,000 particles in total in a simulation box with linear dimension of 205 particle diameters in x and y directions. Both systems have therefore a number density of 1.2. Results are reported in reduced units where $\sigma_{AA} \equiv \sigma$ and ϵ_{AA} the unit of energy. For both 2D and 3D systems, we first run 100,000 time steps at temperature $T=1$ followed by a quench to $T \approx 0$ in 10 million time steps with a time step of $0.005 \tau_{LJ}$ using a dissipative particle dynamics (DPD) thermostat. The NVE ensemble is used throughout the subsequent simulations. At each temperature, we use the saved configurations during the quench, run another 100,000 time steps to further relax the system at the desired temperature followed by another run during which data is taken and configurations are saved in order to be used in the GDyNets.

Detection of elementary particle hops. To capture the rearrangements in the form of discrete hops or jumps, snapshots of simulation data were saved every $20\tau_{LJ}$ and were input to algorithm. For each particle, time windows containing $N_{hist} = 10$ frames of the trajectory were passed to the algorithm. The algorithm divides this evaluation time window into two time windows $A[t, t+N_{hist}/2)$ and $B[t+N_{hist}/2, N_{hist})$, and a hop identifier parameter is then calculated at time t using:

$$p_{hop}(t) = \sqrt{\langle (r_A - \bar{r}_B)^2 \rangle \cdot \langle (r_B - \bar{r}_A)^2 \rangle} \quad (15)$$

which is a measure of average distance between the mean position of the particle in time window A, \bar{r}_A , and all trajectory points in time window B, r_B , and vice versa. The algorithm is therefore useful to filter out thermal fluctuations and $p_{hop}(t)$ shows strong peaks during rearrangements [31]. A threshold value of $p_{th} = 0.5$ was chosen to record the time of rearrangements.

Acknowledgements

We thank Ludovic Berthier and Céline Ruscher for insightful comments on the manuscript. This work was supported by the Natural Sciences and Engineering Research Council of Canada (NSERC). Computing resources were provided by ComputeCanada.

Data availability

The data associated with this research is available upon request.

Author contributions

All authors were equally involved in conception of the research project. S.S. performed all calculations, provided initial analysis and the first draft of the manuscript. All authors equally contributed to discussing results and to writing the manuscript.

Competing interests

The authors declare no competing interests.

Correspondence and requests for materials should be addressed to S.S.

- [1] L. Berthier and G. Biroli, Theoretical perspective on the glass transition and amorphous materials, *Reviews of modern physics* **83**, 587 (2011).
- [2] A. Widmer-Cooper, H. Perry, P. Harrowell, and D. R. Reichman, Irreversible reorganization in a supercooled liquid originates from localized soft modes, *Nature Physics* **4**, 711 (2008).
- [3] C. P. Royall, S. R. Williams, T. Ohtsuka, and H. Tanaka, Direct observation of a local structural mechanism for dynamic arrest, *Nature materials* **7**, 556 (2008).
- [4] R. Candelier, A. Widmer-Cooper, J. K. Kummerfeld, O. Dauchot, G. Biroli, P. Harrowell, and D. R. Reichman, Spatiotemporal hierarchy of relaxation events, dynamical heterogeneities, and structural reorganization in a supercooled liquid, *Physical review letters* **105**, 135702 (2010).
- [5] H. Tanaka, H. Tong, R. Shi, and J. Russo, Revealing key structural features hidden in liquids and glasses, *Nature Reviews Physics* **1**, 333 (2019).
- [6] L. Berthier, Dynamic heterogeneity in amorphous materials, arXiv preprint arXiv:1106.1739 (2011).
- [7] Q. Wang and A. Jain, A transferable machine-learning framework linking interstice distribution and plastic heterogeneity in metallic glasses, *Nature communications* **10**, 1 (2019).
- [8] Q. Wang, J. Ding, L. Zhang, E. Podryabinkin, A. Shapeev, and E. Ma, Predicting the propensity for thermally activated β events in metallic glasses via interpretable machine learning, *npj Computational Materials* **6**, 1 (2020).
- [9] Z.-Y. Yang, D. Wei, A. Zacccone, and Y.-J. Wang, Machine-learning integrated glassy defect from an intricate configurational-thermodynamic-dynamic space, *Physical Review B* **104**, 064108 (2021).
- [10] E. D. Cubuk, S. S. Schoenholz, J. M. Rieser, B. D. Malone, J. Rottler, D. J. Durian, E. Kaxiras, and A. J. Liu, Identifying structural flow defects in disordered solids using machine-learning methods, *Physical Review Letters* **114**, 108001 (2015).
- [11] S. S. Schoenholz, E. D. Cubuk, D. M. Sussman, E. Kaxiras, and A. J. Liu, A structural approach to relaxation in glassy liquids, *Nature Physics* **12**, 469 (2016).
- [12] E. D. Cubuk, S. S. Schoenholz, E. Kaxiras, and A. J. Liu, Structural properties of defects in glassy liquids, *The Journal of Physical Chemistry B* **120**, 6139 (2016).
- [13] S. S. Schoenholz, E. D. Cubuk, E. Kaxiras, and A. J. Liu, Relationship between local structure and relaxation in out-of-equilibrium glassy systems, *Proceedings of the National Academy of Sciences* **114**, 263 (2017).
- [14] S. S. Schoenholz, Combining machine learning and physics to understand glassy systems, in *Journal of Physics: Conference Series*, Vol. 1036 (IOP Publishing, 2018) p. 012021.
- [15] V. Bapst, T. Keck, A. Grabska-Barwińska, C. Donner, E. D. Cubuk, S. S. Schoenholz, A. Obika, A. W. Nelson, T. Back, D. Hassabis, *et al.*, Unveiling the predictive power of static structure in glassy systems, *Nature Physics* **16**, 448 (2020).
- [16] E. Boattini, S. Marín-Aguilar, S. Mitra, G. Foffi, F. Smalenburg, and L. Filion, Autonomously revealing hidden local structures in supercooled liquids, *Nature communications* **11**, 5479 (2020).
- [17] J. Paret, R. L. Jack, and D. Coslovich, Assessing the structural heterogeneity of supercooled liquids through community inference, *The Journal of chemical physics* **152**, 144502 (2020).
- [18] N. G. Van Kampen, *Stochastic processes in physics and chemistry*, Vol. 1 (Elsevier, 1992).
- [19] W. C. Swope, J. W. Pitera, and F. Suits, Describing protein folding kinetics by molecular dynamics simulations. 1. theory, *The Journal of Physical Chemistry B* **108**, 6571 (2004).
- [20] J.-H. Prinz, H. Wu, M. Sarich, B. Keller, M. Senne, M. Held, J. D. Chodera, C. Schütte, and F. Noé, Markov models of molecular kinetics: Generation and validation, *The Journal of chemical physics* **134**, 174105 (2011).
- [21] B. E. Husic and V. S. Pande, Markov state models: From an art to a science, *Journal of the American Chemical Society* **140**, 2386 (2018).
- [22] V. A. Voelz, G. R. Bowman, K. Beauchamp, and V. S. Pande, Molecular simulation of ab initio protein folding for a millisecond folder nt19 (1- 39), *Journal of the American Chemical Society* **132**, 1526 (2010).
- [23] F. Noé and F. Nuske, A variational approach to modeling slow processes in stochastic dynamical systems, *Multiscale Modeling & Simulation* **11**, 635 (2013).
- [24] A. Mardt, L. Pasquali, H. Wu, and F. Noé, Vampnets for deep learning of molecular kinetics, *Nature communications* **9**, 5 (2018).
- [25] T. Xie, A. France-Lanord, Y. Wang, Y. Shao-Horn, and J. C. Grossman, Graph dynamical networks for unsupervised learning of atomic scale dynamics in materials, *Nature communications* **10**, 2667 (2019).
- [26] A. Stukowski, Visualization and analysis of atomistic simulation data with ovito—the open visualization tool, *Modelling and Simulation in Materials Science and Engineering* **18**, 015012 (2009).
- [27] M. H. Cohen and G. Grest, Liquid-glass transition, a free-volume approach, *Physical Review B* **20**, 1077 (1979).
- [28] A. Widmer-Cooper, P. Harrowell, and H. Fynewever, How reproducible are dynamic heterogeneities in a supercooled liquid?, *Physical review letters* **93**, 135701 (2004).
- [29] R. L. Jack, A. J. Dunleavy, and C. P. Royall, Information-theoretic measurements of coupling between structure and dynamics in glass formers, *Physical review letters* **113**, 095703 (2014).
- [30] R. Candelier, O. Dauchot, and G. Biroli, Building blocks of dynamical heterogeneities in dense granular media, *Phys. Rev. Lett.* **102**, 088001 (2009).
- [31] A. Smessaert and J. Rottler, Distribution of local relaxation events in an aging three-dimensional glass: Spatiotemporal correlation and dynamical heterogeneity, *Physical Review E* **88**, 022314 (2013).
- [32] C. Zhang, L. Hu, Y. Yue, and J. C. Mauro, Fragile-to-strong transition in metallic glass-forming liquids, *The Journal of chemical physics* **133**, 014508 (2010).
- [33] K. Lad, N. Jakse, and A. Pasturel, Signatures of fragile-to-strong transition in a binary metallic glass-forming liquid, *The Journal of chemical physics* **136**, 104509 (2012).
- [34] F. Nuske, B. G. Keller, G. Pérez-Hernández, A. S. Mey, and F. Noé, Variational approach to molecular kinetics, *Journal of chemical theory and computation* **10**, 1739

- (2014).
- [35] F. Noé, Machine learning for molecular dynamics on long timescales, in *Machine Learning Meets Quantum Physics* (Springer, 2020) pp. 331–372.
- [36] T. Xie, A. France-Lanord, Y. Wang, Y. Shao-Horn, and J. C. Grossman, Graph dynamical networks for unsupervised learning of atomic scale dynamics in materials, <https://github.com/txie-93/gdynet/blob/master/notebooks/visualization.ipynb> (2019).

Supplementary Information: Exploring Glassy Dynamics With Markov State Models From Graph Dynamical Networks

Siavash Soltani,¹ Chad W. Sinclair,¹ and Jörg Rottler^{2,3}

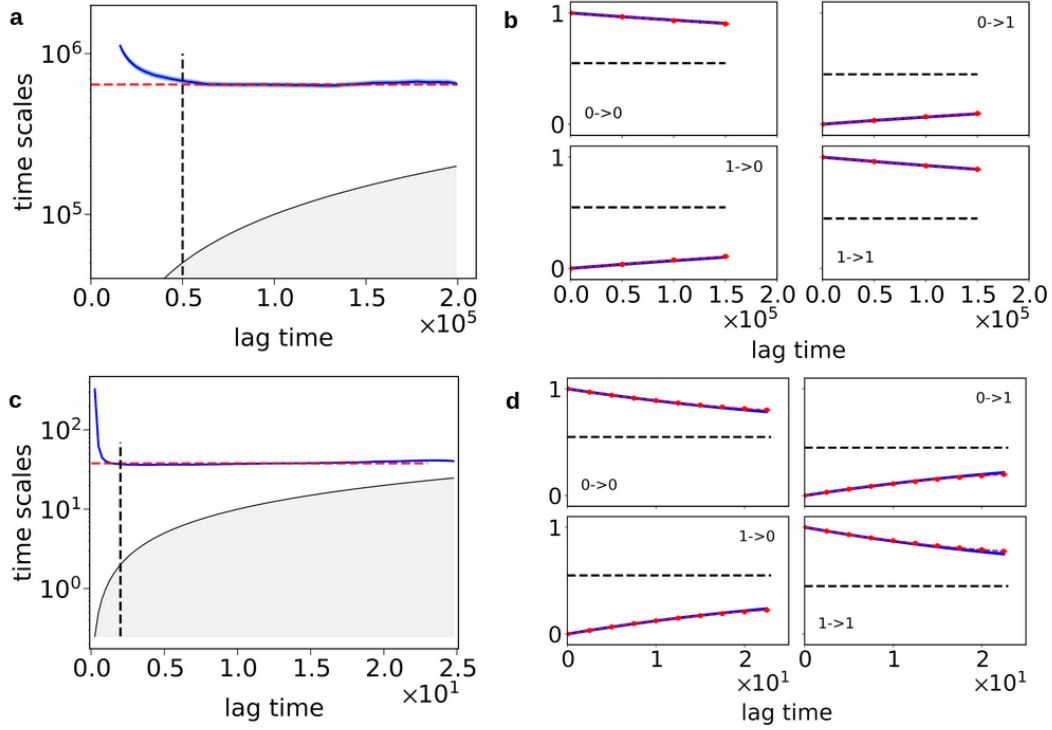
¹*Department of Materials Engineering, The University of British Columbia, Vancouver, BC, Canada V6T 1Z4*

²*Department of Physics and Astronomy, The University of British Columbia, Vancouver, BC, Canada V6T 1Z1*

³*Stewart Blusson Quantum Matter Institute, The University of British Columbia, Vancouver, BC, Canada V6T 1Z4*

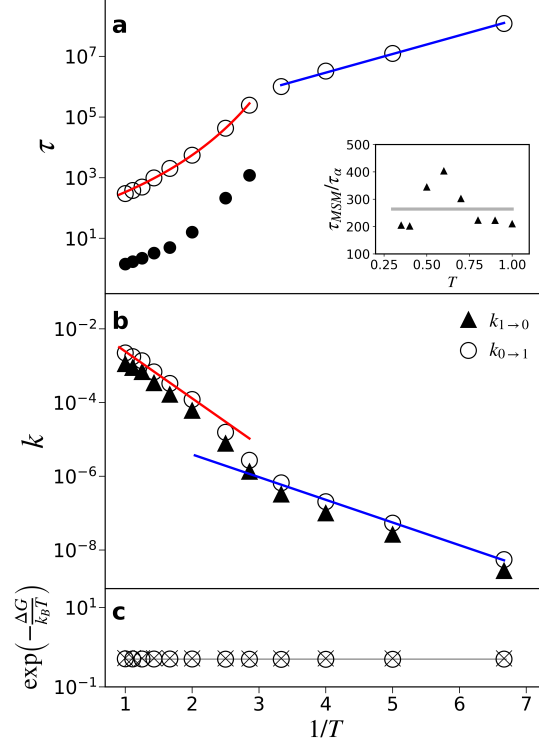
SUPPLEMENTARY NOTES

Supplementary Note 1: Generation and validation of Markov state models. In Supplementary Figure 1 we show the steps used to extract the Markov state time scale and validate the model from the trajectories for two temperatures $T=0.35$ and $T=1$ in the 3D system. Since the states of particles are known, we can construct the transition matrix as a function of lag time and estimate the relaxation time of the model using Equation (1) in the main text. Supplementary Figures 1(a) and 1(c) show the timescale of the Markov state model as a function of lag time. The time scale becomes independent of lag time at large enough lag times and converges to a constant value (red dotted lines), indicating that the model is now Markovian, i.e. the relaxation time does not depend on lag time. We then use the lag time (black dotted lines in (a) and (c)) to construct the transition matrix and validate the Markov model with the CK test, see Equation (10). Figures (b) and (d) show this test, where the blue curves are the components of $K^n(\delta t)$ constructed at the convergence lag time and the red data points are the components of $K(n\delta t)$.



Supplementary Figure 1. Validation of Markov state models. Relaxation time as a function of lag time at **a** $T=0.35$ and **c** $T=1$. The shaded areas are obtained by averaging over 10 sets of particles by randomly dividing them in the test data. CK tests at **b** $T=0.35$ and **d** $T=1$.

Supplementary Note 2: Two-dimensional glass model. We now present the results for the 2D 65-35 Lennard Jones mixture. In Supplementary Figure 2 we show the relaxation timescales, the ‘forward’ and ‘backward’ reaction rates $k_{0 \rightarrow 1}$ and $k_{1 \rightarrow 0}$, and the free energy difference between equilibrium states. The rates almost trace each other again similar to the behaviour observed in the 3D system. An Arrhenius fit to the high temperature regime reveals an activation barrier of 2.92, together with a preexponential factor $\tau_0 \approx 20$. Deep in the glassy state, the barrier becomes temperature independent again at 1.41, with a preexponential time of about 15000.

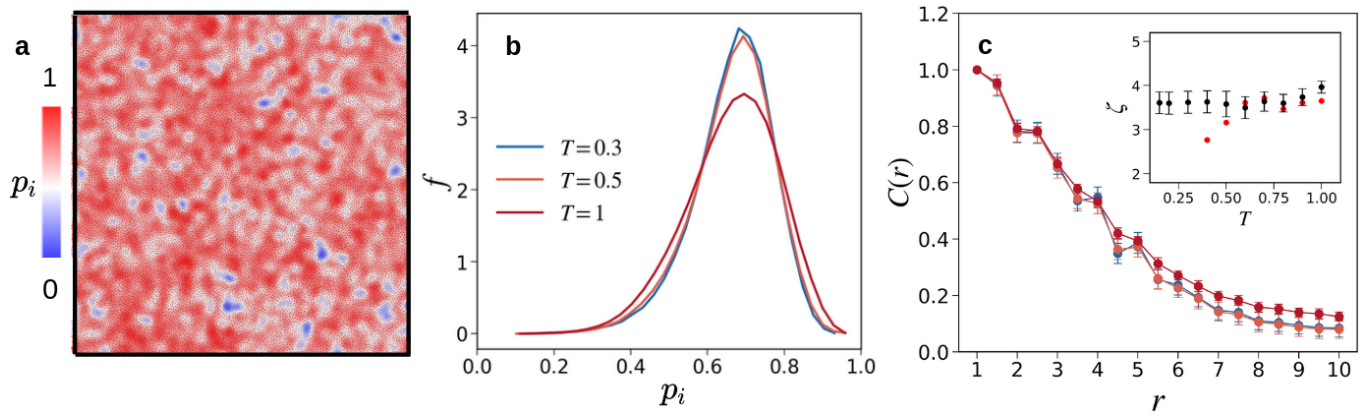


Supplementary Figure 2. Relaxation times, forward and backward reaction rates and free energies obtained using Markov state model. **a** Markov state relaxation times (empty circles) and α relaxation time (filled circles) as a function of inverse temperature. Red solid curve shows a Vogel-Fulcher-Tammann fit $\tau \sim e^{\frac{A}{T-T_0}}$ of the data for $T \geq 0.4$. The obtained T_0 values is 0.17. Arrhenius fit at low temperatures are also shown with blue solid line. **b** Forward and backward rates, $k_{0 \rightarrow 1}$ and $k_{1 \rightarrow 0}$, obtained using equations (1) and (2). **c** Free energy difference between states (circles). \times symbols show $\exp(-\Delta S/k_B)$.

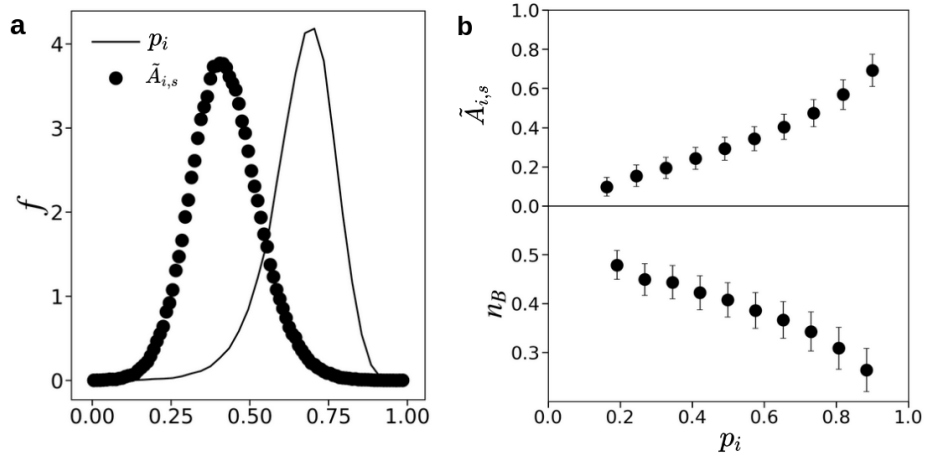
Supplementary Figure 3 shows the analysis on the structure of the state map for the 2D system. The probability distribution of the state map and the correlation length of the state map are again almost temperature independent, similar to the 3D system. However, in the 2D system we observe larger correlation lengths in the state map, between 3 to 4 particle diameters.

Supplementary Figure 4 illustrates the correlation between the state map and the coarse-grained Voronoi areas of majority particles in the 2D system. For smoothing the Voronoi area, we average the Voronoi area of a particle with Voronoi volume of its neighbors within $r = \zeta$. The Pearson correlation factor between the state map and the coarse-grained Voronoi area was found to be 0.81. The values are scaled via Equation 8 to compare the distribution with the state map probability distribution, see Supplementary Figure 4(a).

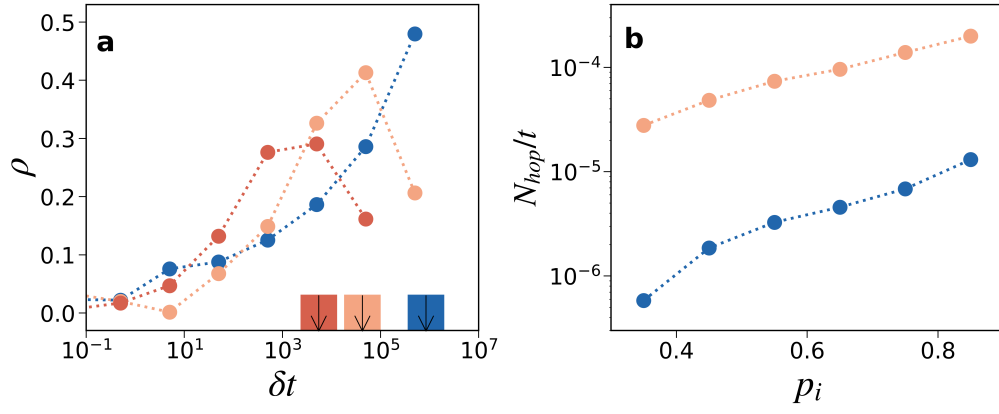
Supplementary Figure 5 analyzes the relationship between the states of the Markov model assigned to individual atoms and the dynamic propensity or the average rate or rearrangements as expressed by the rate of particle hops.



Supplementary Figure 3. Structural analysis of state maps of the 2D system. **a** Example of the state map for a snapshot at $T = 0.3$. **b** The probability distribution of majority particles being in state 0 of particles at 3 different temperatures. Distributions are averaged over 100 equally spaced snapshots of the trajectory. **c** Normalized spatial correlation functions $C(r) = \langle \delta p(0) \delta p(r) \rangle \langle \delta p(0) \delta p(r_{min}) \rangle$ of the state maps at same temperatures as in panel (b). Measurements are obtained using 5 different quench realizations to desired temperatures and an isothermal equilibration of 50,000 LJ time. The snapshot at the end of this equilibration period is then used to extract the data points in **c**. The error bars show the standard error of the mean. Black symbols in inset show the correlation length of the state map, ζ , calculated using Equation 5 in text. Red symbols represent the RMSD of all particles at $t = \tau_{MSM}$. Error bars in the inset show the standard error of the mean of the correlation length of 5 quench realizations.



Supplementary Figure 4. **a** Comparison between the distribution of states and smoothed and scaled Voronoi area (Equation 8) of majority particles in the 2D glass. **b** Correlation between $\tilde{A}_{i,s}$ and number density of minority (B) particles versus state probability.



Supplementary Figure 5. **a** Pearson correlation coefficient between state map and dynamic propensity at $T=0.3, 0.4$, and 0.5 from dark blue to red. The state map is obtained using the snapshot immediately after quench, and the propensity is evaluated as a function of lag time δt from this snapshot. Arrows at the bottom show the MSM time scale each temperature. **b** Average number of hops per unit time vs. the state variable for two different temperatures, $T=0.3, 0.4$. Jump rates are normalized with respect to the overall state probability distributions.